International Journal of Solids and Structures 54 (2015) 147–155

Contents lists available at ScienceDirect

International Journal of Solids and Structures

journal homepage: www.elsevier.com/locate/ijsolstr

Rate dependent finite strain constitutive modeling of polyurethane and polyurethane–clay nanocomposites

Trisha Sain [a,*], Julien Meaud [a,f], Bongjun Yeom [c], Anthony M. Waas [a,b], Ellen M. Arruda [a,d,e]

[a] Department of Mechanical Engineering, University of Michigan, Ann Arbor 48109, USA
[b] Department of Aerospace Engineering, University of Michigan, Ann Arbor 48109, USA
[c] Department of Chemical Engineering, University of Michigan, Ann Arbor 48109, USA
[d] Department of Biomedical Engineering, University of Michigan, Ann Arbor 48109, USA
[e] Macromolecular Science and Engineering, University of Michigan, Ann Arbor 48109, USA
[f] Georgia Institute of Technology, Atlanta, GA, USA

ARTICLE INFO

Article history:
Received 11 March 2014
Received in revised form 20 October 2014
Available online 15 November 2014

Keywords:
Polymer–clay nanocomposite
Constitutive model
Rate dependent
Finite deformation
Viscoplasticity
Frequency sweep

ABSTRACT

A finite strain nonlinear viscoplastic constitutive model for polyurethane (PU)–Montmorillonite clay (MTM) nanocomposites is developed with the goal of characterizing the mechanical response under different strain rates and strain amplitudes. In this model, both the elastic and viscous responses are considered to be nonlinear. It is shown that a simple mathematical extension of the model used to characterize the PU determines the nonlinear material constants for the PU–MTM. A finite deformation nonlinear viscoelastic model is used to represent the mechanical behavior of PU. The rate dependent viscous behavior and multiple relaxation times present in the PU response are determined using the frequency dependent $\tan\delta$ measurements from Dynamic Mechanical Analysis (DMA). The model is capable of accurately capturing both the rate dependent behavior and frequency dependent damping of PU. The entire rate dependent hysteresis behavior (loading–unloading) is predicted accurately through the constitutive model for strains up to 10%. For the PU–MTM nanocomposite, the constitutive stress update is implemented in a finite element (ABAQUS/Explicit) framework and validated using a range of experimental results. The model predictions show excellent agreement with experimental results in capturing rate dependent loading/unloading responses for both PU and PU–MTM nanocomposites. The proposed model can easily be extended to characterize other polyurethane based nanocomposites.

Published by Elsevier Ltd.

1. Introduction

Polymer–clay nanocomposites are used in numerous applications ranging from automobile bumpers to advanced opto-electronic devices. Recent experimental results demonstrate that polymer nanocomposites can exhibit significant property improvements compared to the base polymer. These properties include increased strength, modulus, thermal stability and electrical conductivity (Ramanathan et al., 2005; Sandler et al., 1999; Muzny et al., 1996; Coleman et al., 2004; Podsiadlo et al., 2007). A recent review of the state of the art of polymer–clay nanocomposites (Nguyen and Baird, 2006) has a good discussion of the preparation of such materials and their structure–property relationships. Research is being conducted on developing analytical and numerical models to understand the chemistry, morphology and synergistic effects between nanoparticles and polymer matrices. Recently, many studies have been directed at understanding the effect of an interphase region that is formed in the vicinity of nanoscale fillers (Li et al., 2011a,b; Liu and Brinson, 2006; Sheng et al., 2004). Continuum based finite element modeling studies can be effectively used to understand the physical and mechanical interactions between the nanoparticles and the bulk polymer chains in these nanocomposites (Kaushik et al., 2011; Kheng et al., 2010). As a polymer, the response of bulk polyurethane depends on the applied strain rate and strain amplitude and the dependence can be highly nonlinear. Polyurethanes exhibit a two-phase microstructure composed of soft segments (amorphous phase) and hard segments (semi-crystalline glassy phase). These microstructures can be incorporated into a fully 3D constitutive model as developed in Boyce et al. (1988). Since

* Corresponding author at: Department of Mechanical Engg., North Carolina A & T State University, Greensboro, NC 27410, USA.
E-mail address: tsain@ncat.edu (T. Sain).

http://dx.doi.org/10.1016/j.ijsolstr.2014.10.027
0020-7683/Published by Elsevier Ltd.

polymer chains undergo large stretching, most of the mathematical development is focused on capturing the large strain or post yielding response of the polymers (Arruda et al., 1995; Qi and Boyce, 2005; Bergstrom and Boyce, 1998; Mulliken and Boyce, 2006; Shim and Mohr, 2011). Further, some models focus only on capturing the loading response at different strain rates; however it is extremely important to accurately characterize the unloading response of the polymer in order to capture the dissipation as done in Anand and Gurtin (2003), Anand (1996, 2003). The missing link in the existing state of the art in modeling of polymer constitutive response is to develop a single model which can predict *both*, the rate dependent loading and unloading behavior, together with the amplitude dependent nonlinear response. To predict the viscous dissipation in polyurethane (or such materials) as a function of varying strain rate, the development of a constitutive model which captures the hysteresis response in polymers is necessary. The phenomenon becomes more demanding for PU–MTM nanocomposites, as the stress–strain response in general for these materials is highly nonlinear. In the present paper, a phenomenological constitutive model is proposed for polyurethane (PU) and polyurethane based MTM clay nanocomposites to fill this missing link. The model is shown to capture the amplitude dependent nonlinear response of the PU and the PU–MTM nanocomposite from quasi-static to the moderate strain rate regime. In order to incorporate the rate dependent variation of stiffness and viscous behavior of the polymer the relaxation response is assumed to be a collection of discrete relaxation spectra with several characteristic relaxation times. This approach has been earlier used by Lion (1998), Haupt et al. (2000) to identify the various relaxation times present within a polymer system. In particular, (Lion, 1998), with 4 different relaxation constants and use of the experimental storage modulus was found to be good enough to predict frequency dependent variation of loss modulus, but amplitude dependence was not estimated correctly. In another work (Haupt et al., 2000) the continuous relaxation spectra was approximated through a series of step functions and parameters were estimated with help of a fractional derivative based model. However the method was not used for capturing amplitude dependent nonlinear response of the polymer. The present approach considers the frequency dependent tan δ data to characterize the multiple relaxation processes in the PU system. The tan δ involves both the storage (stiffness) and loss modulus (viscosity) in characterizing the relaxation behavior. The proposed model captures the loading path of the constitutive response at different rates, and effectively predicts the unloading response. The mathematical framework is based on the commonly used concept of characterizing the various rate activated relaxation processes through discrete approximations. This approach is shown to be able to capture the PU–MTM nanocomposite response. In particular, the approach is able to predict rate dependent responses at strain rates higher than those corresponding to the highest frequency of the DMA apparatus (100 Hz). The constitutive framework for PU–MTM nanocomposites is developed considering PU as a constituent and hence the PU parameters are directly fed into the nanocomposite models in addition to incorporating the combined effects of clay and interphase. The successful implementation of the nanocomposite model greatly depends on how well the base PU is characterized, hence considerable attention is paid to validation of the PU model. Samples of two different volume fractions of clay are used $f = 4\%$ and $f = 9\%$ for the present study. The proposed constitutive model is implemented in a finite element framework and is shown to predict the stress–strain response of PU and PU–MTM nanocomposites with good accuracy.

2. Constitutive polymer model

2.1. Experimental characterization of PU

The polymer chosen is a polyurethane (manufactured in-house) and has a storage modulus of 40 MPa and very high damping ($\tan\delta = 0.98$ at 1 Hz) at room temperature. The pristine PU is experimentally characterized through uniaxial loading–unloading tests at different rates ($0.5\%/\sec - 10\%/\sec$), stress relaxation tests, and Dynamic Mechanical Analysis (DMA).

Stress relaxation tests performed at three different strain levels ($1\%, 2\%, 5\%$) and the normalized modulus as a function of time is plotted in Fig. 1 which shows that PU is not an ideal linear viscoelastic material as for a linear viscoelastic material the normalized relaxation modulus plots at different strain coincide with each other; however the nonlinearity may be limited to entropic elasticity, which appears in the long term modulus. Hence a nonlinear spring is added to the standard linear viscous solid framework as shown in the schematic representation of the model in Fig. 2.

2.2. Mathematical formulation of the constitutive model

As seen in Fig. 2 the model consists of several Maxwell branches spring and dashpot combinations to represent the discrete relaxation spectrum, each of them with a characteristic relaxation time τ_i. The number of Maxwell branches can vary to capture the rate dependent response of the PU. The nonlinear spring is added to capture the nonlinear elastic response at large strains. The macroscopic deformation gradient **F** is the same in all branches and is given by:

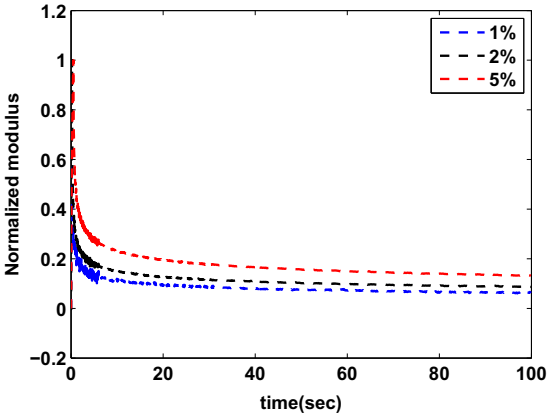

Fig. 1. Normalized relaxation modulus at various strain levels for polyurethane.

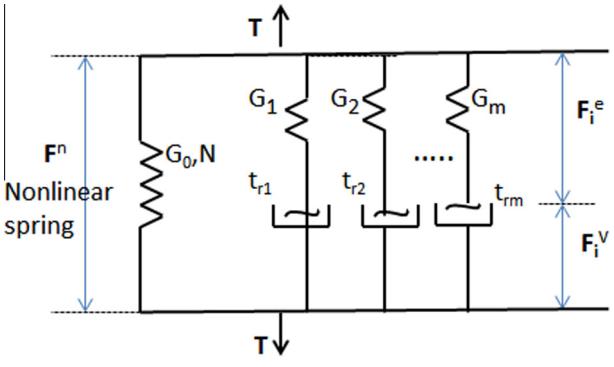

Fig. 2. Schematic representation of the constitutive model for polyurethane.

$$\mathbf{F} = \mathbf{F}^n = \mathbf{F}_i, \quad i = 1, m \tag{1}$$

where the superscript n represents the nonlinear spring branch and the subscript i stands for the ith spring and dashpot branch, and m is the total number of Maxwell branches. The total Cauchy stress is the sum of the stresses from all the springs, and is expressed as,

$$\mathbf{T} = \mathbf{T}^n + \sum_{i=1}^{m} \mathbf{T}_i^e \tag{2}$$

where the $\mathbf{T}_i^e$ are the stresses in the Maxwell springs. The Cauchy stress in the non linear spring following the eight chain potential (Arruda and Boyce, 1993) is given as:

$$\mathbf{T}^n = \frac{n_1 k\theta}{3J} \frac{\sqrt{N}}{\lambda_{chain}} L^{-1}\left(\frac{\lambda_{chain}}{\sqrt{N}}\right)\overline{\mathbf{B}}' \tag{3}$$

with n_1 being the chain density (number of molecular chains per unit reference volume) of the underlying macromolecluar network, k the Boltzmann's constant, θ the absolute temperature, currently taken as constant at room temperature and $J = det(\mathbf{F})$. N represents the length of the chains in the polymer network and $\sqrt{N}$ represents the limiting stretch of each chain. Concisely $G_0 = n_1 k\theta$, the rubbery modulus or initial stiffness of the nonlinear spring as shown in Fig. 2.

In Eq. (3), $\overline{\mathbf{B}}$ is the isochoric left Cauchy–Green strain given by

$$\overline{\mathbf{B}} = \overline{\mathbf{F}}\overline{\mathbf{F}}^T \tag{4}$$

and $\overline{\mathbf{B}}'$ is the deviatoric component of $\overline{\mathbf{B}}$ as given by,

$$\overline{\mathbf{B}}' = \overline{\mathbf{B}} - tr(\overline{\mathbf{B}}/3) \tag{5}$$

The isochoric deformation is developed by neglecting the volume change as:

$$\overline{\mathbf{F}} = J^{-1/3}\mathbf{F} \tag{6}$$

In Eq. (3), L^{-1} is the inverse Langevin function, given by its Padé approximation,

$$L^{-1}(\xi) = \xi\frac{3 - \xi^2}{1 - \xi^2} \tag{7}$$

and (3), λ_{chain} is the stretch on each chain in the network as given by $\lambda_{chain} = \sqrt{I_1/3}$, with $I_1 = tr(\overline{\mathbf{B}})$, the first invariant of $\overline{\mathbf{B}}$.

2.3. Kinematics of the Maxwell Elements

The kinematics of each Maxwell spring–dashpot element assumes that the total deformation gradient can be multiplicatively decomposed into an elastic part $\mathbf{F}_i^e$ and a viscous part $\mathbf{F}_i^v$ as:

$$\mathbf{F} = \mathbf{F}_i^e\mathbf{F}_i^v \tag{8}$$

Furthermore, we introduce the relations among the velocity gradient l_i, the rate of total deformation tensor and the rate of viscous strain tensor (in the current configuration) as follows,

$$\mathbf{l} = \dot{\mathbf{F}}\mathbf{F}^{-1} = \dot{\mathbf{F}}_i^e\mathbf{F}_i^{e-1} + \mathbf{F}_i^e.\left(\dot{\mathbf{F}}_i^v\mathbf{F}_i^{v-1}\right)\mathbf{F}_i^{e-1} \tag{9}$$

Hence, in the elastically unloaded configuration, the viscoplastic velocity gradient can be written as,

$$\mathbf{l}^v = \mathbf{D}_i^v + \mathbf{W}_i^v = \dot{\mathbf{F}}_i^v\mathbf{F}_i^{v-1} \tag{10}$$

where $\mathbf{D}_i^v$ is the rate of viscous strain and $\mathbf{W}_i^v$ is the viscous spin tensor respectively. Without loss of generality, assuming the constitutive model to be isotropic one can assume the viscous spin to be zero ($\mathbf{W}_i^v = 0$) and the viscous flow rule is expressed as

$$\mathbf{D}_i^v = \frac{\dot{\gamma_{di}}^v}{\sqrt{2}\tau_{vi}}\mathbf{T}_i^{e\prime} + \frac{\dot{\gamma_{Pi}}^v}{\sqrt{2}\tau_{vi}}P_i\mathbf{I} \tag{11}$$

where P_i is the hydrostatic pressure. In most models, the viscous stretch rate is assumed to depend only on the deviatoric component of the driving Cauchy stress (the first term in the right hand side of Eq. (11)). However we found it necessary to include a small component that depends on the hydrostatic pressure in the viscous stretch rate in order to fit the DMA data (the 2nd term in the right hand side of Eq. (11)). The ith equivalent stress $(\overline{\tau_v})_i$ is given by

$$(\overline{\tau_v})_i = \left[\frac{1}{2}\mathbf{T}_i^{e\prime}\mathbf{T}_i^{e\prime}\right]^{1/2} \tag{12}$$

where $\mathbf{T}_i^{e\prime}$ is the deviatoric component of the Cauchy stress developed in the spring connected in series with the ith dashpot. The constitutive equation to describe the stress–strain response in the ith spring is given by

$$\mathbf{T}_i^e = \frac{1}{(det\mathbf{F}_i^e)}\mathbf{L}_i^e(ln\mathbf{V}_i^e) \tag{13}$$

where $\mathbf{V}_i^e$ is the left stretch tensor obtained by polar decomposition of the elastic deformation gradient as

$$\mathbf{F}_i^e = \mathbf{V}_i^e\mathbf{R}_i^e \tag{14}$$

and $\mathbf{L}_i^e$ is the fourth order elasticity tensor of the ith spring and given by,

$$\mathbf{L}_i^e = \lambda\mathbf{I}\otimes\mathbf{I} + 2\mu\mathcal{I}_{sym} \tag{15}$$

where λ and μ are the Lame parameters $\mathbf{I}$ is the second order identity tensor and $\mathcal{I}_{sym}$ is the symmetric part of the 4th order tensor. In Eq. (11), $\dot{\gamma_{di}}^v$ and $\dot{\gamma_{Pi}}^v$ are the equivalent viscous strain rates due to the deviatoric stress and due to the hydrostatic pressure respectively, and are assumed to follow a linear viscous law. Moreover, the viscous laws for deviatoric and volumetric deformations are assumed to have the same relaxation time constant, t_{ri}. For a linear viscoelastic model, the relationship between the strain rate and the stress in the linear small strain regime is given by

$$\dot{\epsilon} = \frac{dev(\mathbf{T}_i^e)}{2Gt_{ri}} + \frac{tr(\mathbf{T}_i^e)}{3Kt_{ri}} \tag{16}$$

In order for the finite deformation model to be equivalent to a linear viscoelastic model described by Eq. (16) in the small strain regime, the equivalent viscous strain rates are given by:

$$\dot{\gamma_{di}}^v = \frac{\sqrt{2}(\overline{\tau_v})_i}{2G_i t_{ri}} \tag{17}$$

$$\dot{\gamma_{Pi}}^v = \frac{\sqrt{2}(\overline{\tau_v})_i}{3K_i t_{ri}} \tag{18}$$

where G_i (K_i) is the shear modulus (bulk modulus) corresponding to the ith elastic spring. As the polymers are nearly incompressible materials with $K \gg G$, the dissipation due to the hydrostatic term is essentially negligible compared to the shear dissipation. The procedure to determine the material constants is explained in the following section.

2.4. Equivalent prony series model: characterizing strain rate/frequency dependent behavior of polyurethane

In order to characterize the rate dependent behavior of PU, the relaxation behavior is approximated as a combination of several discrete relaxation spectra. Hence an equivalent frequency domain approximation for the complex shear and bulk modulus can be written in terms of a Prony series expansion. For a linear viscoelastic material, in response to a sinusoidal load of frequency ω (in radians), the complex shear modulus, $G^*(\omega)$, and the complex bulk modulus, $K^*(\omega)$, can be written as:

$$G^*(\omega) = G_0 + \sum_{i=1}^{N_b} \frac{G_i I\omega t_{ri}}{1 + I\omega t_{ri}} \tag{19}$$

$$K^*(\omega) = K_0 + \sum_{i=1}^{N_b} \frac{K_i I\omega t_{ri}}{1 + I\omega t_{ri}} \tag{20}$$

where the superscript $*$ denotes a complex number, I denotes the imaginary unit number, G_0 and K_0 are the initial shear and bulk moduli of the hyperelastic spring, $G_i, i = 1, .., N_b$ are the shear moduli of the elastic springs, $K_i, i = 1, .., N_b$ are the bulk moduli of the elastic springs and t_{ri} are the relaxation times of the dashpots.

Following Eq. (19), the viscoelastic loss factor $(\tan\,\delta)$ can be written as

$$\tan\,\delta = \frac{img(G^*(\omega))}{Re(G^*(\omega))} \tag{21}$$

Hence $\tan\,\delta$ is a function of the G_i and t_{ri}. A least squares fit is performed between the experimental frequency sweep measurement of $\tan\,\delta$ and Eq. (21) to determine the G_i's and t_{ri}'s. To assess the goodness of fit the sum of the squared of the residuals (R^2) is calculated and compared with a user specified tolerance as

$$R^2 = \sum_{i=1}^{M} (\tan\,\delta_i - \tan\,\delta_f)^2 \leqslant \text{tol} \tag{22}$$

where $\tan\,\delta_i$ is the experimentally measured value and $\tan\,\delta_f$ is the fitted value and M represents the total count of data set. In the present study $R^2 \leqslant 0.05$ is considered to be the criterion for a good fit.

2.5. Material parameter identification and validation with experiments

To find the initial shear modulus of the hyperelastic spring $(G_0 = n_1 k\theta)$ and limiting stretch $\sqrt{N}$, stress relaxation experiments as described earlier are performed at three different strain levels. The specimens are loaded to 1%, 2% and 5% strains at a strain rate of 10%/sec and held there for $t = 100$ sec. All springs in series with dashpots will eventually relax and the stress in this relaxed configuration will correspond to the stress in the hyper-elastic spring at that strain level. Hence, the relaxed stress values (27.1 kPa, 64.5 kPa and 153.0 kPa) at those three strain levels $(0.01, 0.02$ and $0.05)$ respectively are used to find the initial stiffness and the limiting stretch of the nonlinear spring by a nonlinear least squares fit to Eq. (3) and found to be 1.115 MPa and 20 respectively. It is to be noted that the nonlinearity in the relaxation response is assumed to be in the elastic response and characterized through this hyperelastic spring. With G_0 found as explained, another least squares fit is performed to determine the G_i's and t_{ri}'s as mentioned in Section 2.4. These simulations involve optimizing the fit to the tan δ versus frequency response as in Fig. 3 (a) with a Prony series containing $N_b = 1$ to $N_b = 5$ terms. Fig. 3 (a) shows that $N_b < 5$ deviates significantly from the data and $N_b = 5$ provides an excellent $(R^2 = 0.0342)$ match between the computed and experimental tan δ. The relaxation times and moduli for the $N_b = 5$ branches are reported in Table 1 in decreasing order of time constants.

Table 1
Material parameters for polyurethane.

i	1	2	3	4	5
t_{ri} (sec)	22.95	1.12	0.16	0.023	0.0023
G_i (MPa)	1.85	4.04	15.04	43.28	107.45
$G_0 = n_1 k\theta$	1.115 MPa				
N	20				

The effect of all the relaxation times on the loading/unloading response of PU is examined via a constitutive update which includes the finite deformation formulation, written in the commercial finite element (FE) package ABAQUS/Explicit using a VUMAT. FE simulations are performed to predict material response at different strain rates. Fig. 3 (b) shows the FE simulation results for the quasi-static loading case predicted with an increasing number of Prony series terms and compared with experiment. The experimental stress–strain responses at different strain rates are obtained by uniaxial tensile testing in a standard MTS machine. By comparing all the relaxation times in Table 1 it is clear that the stiffness corresponding to the slowest relaxation time of $t_{r1} = 22.95$ sec will have a significant effect on the quasi-static $(0.5\%/\text{sec})$ loading case, as the total time of loading for 10% strain is $t_L = 0.1/0.005 = 20$ sec. To incorporate the viscous effects seen in the material response, the relaxation constants that are faster than the loading time but still have a significant effect within the time scale analyzed need to be included. It is observed that the 1st three terms are sufficient to capture the entire hysteresis loop at 0.5%/sec with reasonable agreement. The relaxation times $\leqslant 0.023$ sec do not improve the goodness of fit at this rate.

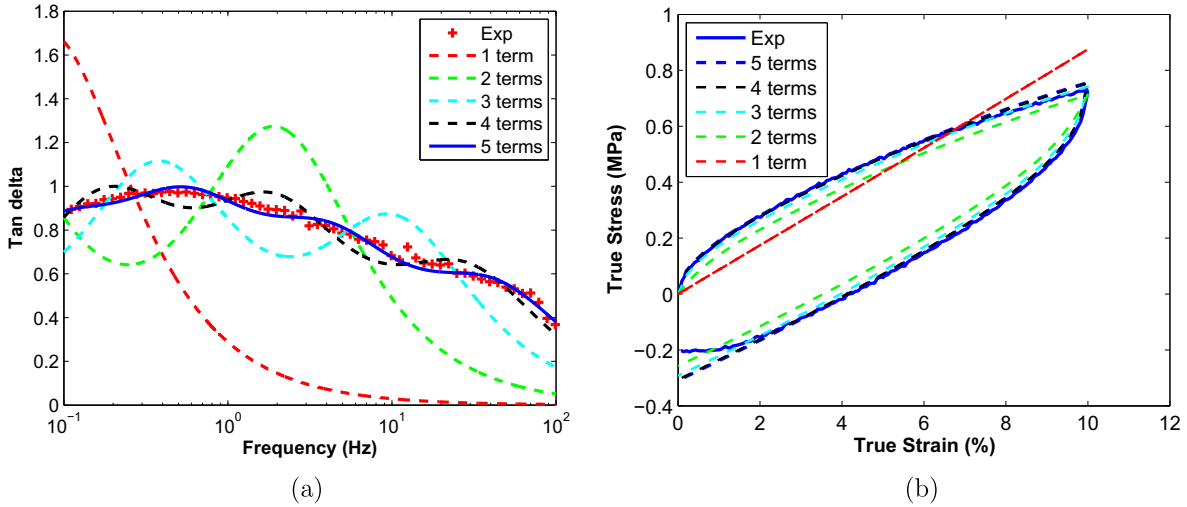

Fig. 3. Effect of number of Prony series terms on (a) *tan* δ as a function of frequency and comparison with experimental data; (b) Uniaxial stress–strain curve for polyurethane at a quasi-static strain rate of $0.5\%/$ sec and effect of the number of Prony series terms on the response.

However the influence of faster relaxation times becomes more prominent as the strain rate of loading increases. As the strain rate increases, longer relaxation time constants become large compared to the duration of the experiment and play less of a role in the viscous dissipation of the material at higher rates. The contributions due to the shorter relaxation times become increasingly important at higher rates. For a material with multiple relaxation times such as the PU discussed here, the rate dependent behavior is essentially a function of multiple relaxation times that are on the order of test duration (Wineman and Rajagopal, 2000).

Hence for polymers with multiple relaxation times, to predict high rate responses accurately it is necessary to include fast relaxation times, which invariably influence the material behavior as seen in Fig. 4(a).

To examine the capability of the model to capture the nonlinear dissipation as a function of strain level, simulations are performed for the quasi-static loading case in which the specimens are loaded and unloaded to different strain levels. Fig. 4 (b) shows an excellent agreement between simulation with ($N_b = 5$) and experimental data at all strain levels. For viscoelastic materials damping not only depends on the strain rate, but also on the strain amplitude and the dependence can be nonlinear in nature; it is noted that the present constitutive approach has the capability of predicting the amplitude dependent hysteresis loss quite well.

3. Constitutive model of PU-based MTM nanocomposites

To predict the constitutive response of PU-based MTM nanocomposites the following assumptions are made:

- The constitutive model considers the nanocomposite system as a combination of bulk polyurethane and a homogenized contribution of clay and interphase. The phenomenological model consists of Maxwell elements corresponding to the polyurethane and additional elements representing the combined effects of the clay and interphase. The nonlinear spring incorporates the combined elasticity of all three constituents.
- Clay is considered to be elastic and the viscous contribution due to the combined effects of clay and the interphase is solely due to the interphase.

In order to determine the stiffness and relaxation constants for the homogenized clay and interphase in the PU–MTM experimental DMA data are used for $f = 4\%$. The response of PU–MTM at $f = 9\%$ is predicted assuming all of the G_i at $f = 4\%$ scale by the same factor as the increase in the clay volume fraction, 2.25. To characterize the nonlinear viscous dashpots, a phenomenological law commonly used for glassy polymers is introduced. Using Argon's (1973) theory of viscoplastic dissipation, which states that the deviatoric part of the viscoplastic strain rate is related to the activation energy of the polymer chain as

$$\dot{\gamma}^{Vv} = \dot{\gamma}_0^{NL} exp\left[-\frac{AS}{k\theta}\left(1-\frac{\overline{\tau}_v}{S}\right)\right] - \dot{\gamma}_0^{NL} exp\left[-\frac{AS}{k\theta}\left(1+\frac{\overline{\tau}_v}{S}\right)\right] \tag{23}$$

where $\dot{\gamma}_0^{NL}$ is the pre-exponential factor proportional to the attempt frequency and S is the athermal shear strength with an initial value of $S_0 = \frac{0.077G}{(1-\nu)}$, related to the elastic shear modulus G and the Poisson's ratio ν (Argon, 1973; Arruda et al., 1995). A is the zero stress level activation energy, k is the Boltzmann's constant and θ is the absolute temperature. The above described strain rate equation is very commonly used to capture the response of glassy polymers. In large deformation cases, the 2nd term in Eq. (23) is often neglected. In the small strain regime, neglecting the 2nd term can cause non-physical viscous dissipation at zero stress. The viscous strain rate corresponding to hydrostatic pressure is considered to be linear as before (2nd part of Eq. (11)).

3.1. Equivalent linearization of the constitutive model

The DMA measurements on the PU–MTM nanocomposites show a significant variation of storage modulus and damping values as a function of frequency as shown in Fig. 5. Following a similar approach as for PU, the rate dependent material constants (G_i and t_{ri}) are fitted using the frequency dependent tan δ values for $f = 4\%$. However, for purposes of the least squares fit only we have linearized the nonlinear equation to an equivalent linear one by assuming that in the small strain regime linear viscosity prevails. The assumption can be justified by the fact that DMA measurements are done at a very low amplitude strain level 0.1% with a very low pre-strain value (0.5%). Simplifying Eq. (23), we obtain

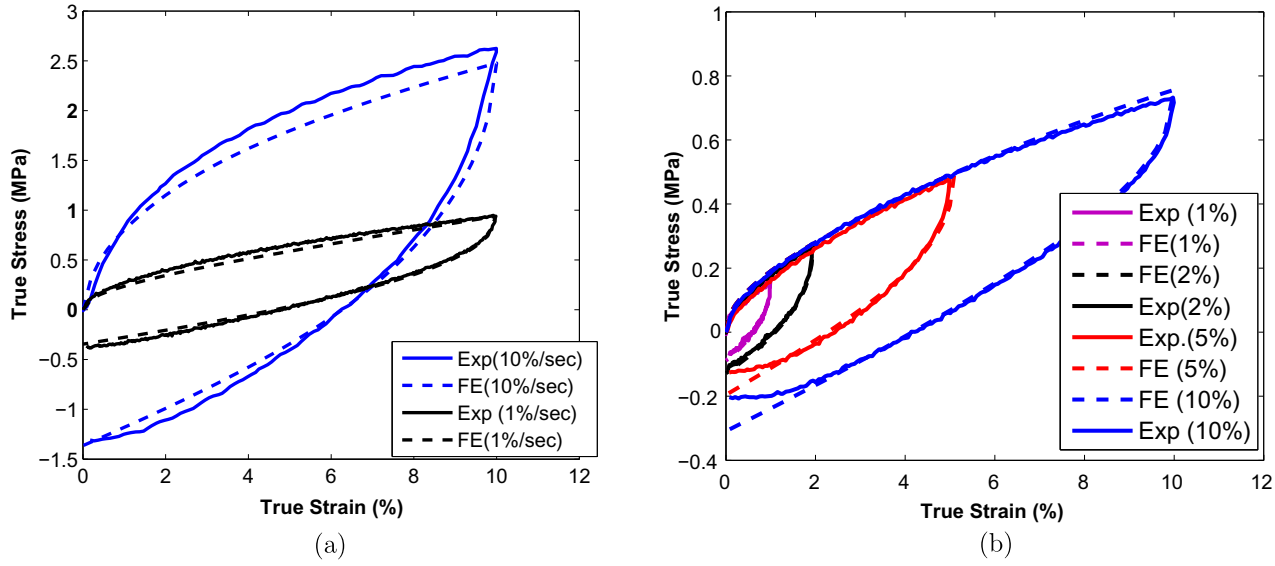

Fig. 4. (a) Uniaxial stress–strain response curves for polyurethane at strain rates (1.0%/*sec*) and (10.0%/*sec*) (b) uniaxial stress–strain curves at quasi static strain rate and various strain levels and FE model predictions using 5 Prony series terms.

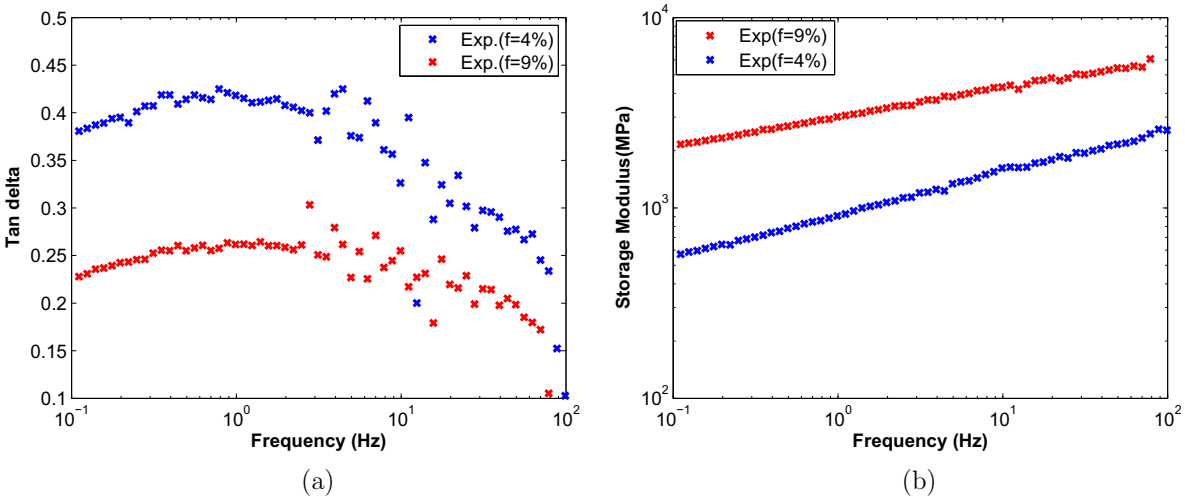

Fig. 5. *tan δ* versus frequency (a) and storage modulus versus frequency (b) response curves for $f = 4\%$ and $f = 9\%$ PU–MTM nanocomposites.

$$\dot{\gamma}^{Vv} = \dot{\gamma}_0^{NL} exp\left(-\frac{AS}{k\theta}\right)\left[exp\left(\frac{A\tau}{k\theta}\right) - exp\left(\frac{-A\tau}{k\theta}\right)\right] \tag{24}$$

Assuming small strains and the corresponding τ to be small, the exponential function can be approximated as $exp\left(\frac{A\tau}{k\theta}\right) = \left(1 + \frac{A\tau}{k\theta}\right)$. Hence one can rewrite Eq. (24) as

$$\dot{\gamma}^{Vv} = \dot{\gamma}_0^{NL} exp\left(-\frac{AS_0}{k\theta}\right)\left(\frac{2A\tau}{k\theta}\right) \tag{25}$$

Equating Eq. (25) with the deviatoric part of the linear viscous relation in Eq. (16), we obtain a relation between the two pre-exponential factors as:

$$\dot{\gamma}_0^{NL} = \frac{\sqrt{2}}{4Gt_r}\frac{k\theta}{A\exp\left(-\frac{AS_0}{k\theta}\right)} \tag{26}$$

The Prony series approximation of the complex modulus results in several (G_i, t_{ri}) pairs. Using those (G_i, t_{ri}) values in Eq. (26), the nonlinear reference viscous strain rate is obtained. The reference values are then substituted in Eq. (23) to compute the nonlinear rate of dissipation under finite deformation. The following section explains the material parameter identification procedure in detail.

4. Material parameter identification and validation of the PU–MTM constitutive model with experiments

In order to determine the material parameters the experimental DMA data for $f = 4\%$ are used. As explained in Section 3, the constitutive framework for the nanocomposite includes PU and the combined effects of interphase and clay. It is assumed that the PU–MTM DMA data contains the information corresponding to bulk PU. To extract the information for the homogenized clay-interphase part, the PU storage modulus and loss modulus are subtracted from the PU–MTM data for $f = 4\%$. A least squares fit is then performed over the tan $\delta = \frac{G_{loss}(PU-MTM)-G_{loss}(PU)}{G_{storage}(PU-MTM)-G_{storage}(PU)}$, to determine the stiffness and relaxation coefficients for the combined clay and interphase. It is seen that 5 terms in the Prony series approximation provides a reasonable match with the experimental data as shown in Fig. 6 with $R^2 = 0.04$.

The parameters estimated for the combined effect of clay and interphase are reported in Table 2 for $f = 4\%$. Analyzing the relative values of t_r, it is known from the PU study that $t_r > 0.1$ sec will have a significant effect on the quasi-static response. Hence the viscous dashpot corresponding to $t_r = 4.435$ sec is considered as nonlinear. The associated parameters for the nonlinear viscous relation are also reported in Table 2. A user material

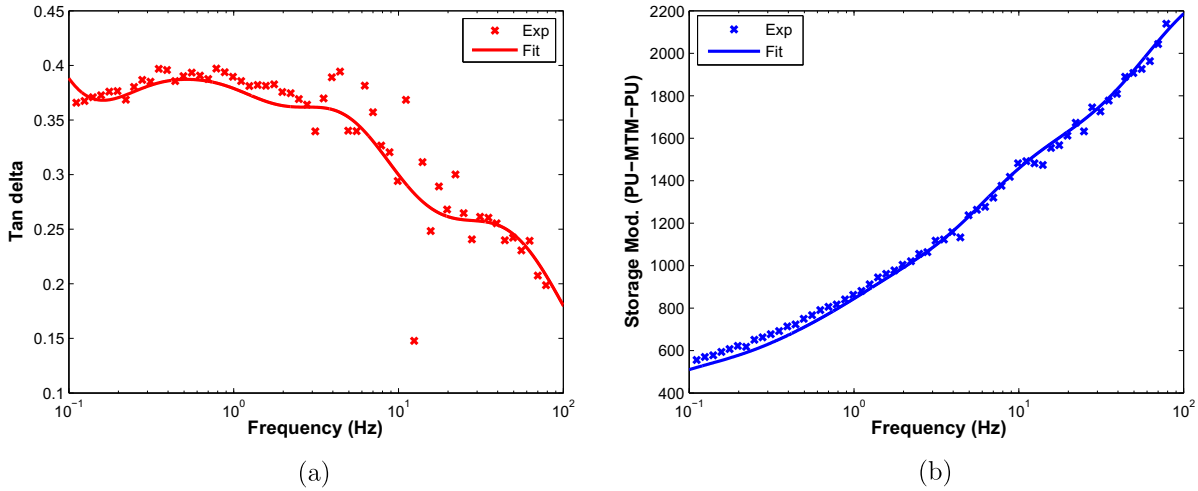

Fig. 6. (a) *tan δ* versus frequency for the combined clay and interphase and (b) storage modulus for the combined clay and interphase versus frequency response curves for $f = 4\%$ PU–MTM nanocomposites.

subroutine (VUMAT) is written in ABAQUS/Explicit for the entire finite deformation constitutive equations and FE simulations are performed to validate the proposed modeling approach. The material subroutine can be used to predict large scale simulations with realistic geometry in finite element environment. Fig. 7 (a) shows the comparison between the model prediction and experiments performed on uniaxial test conditions at a quasi-static strain rate $(0.5\%/\,\mathrm{sec})$ for $f = 4\%$ PU/MTM nanocomposites. The specimens are loaded to a strain level of 5% and 10% followed by unloading. The model results are in excellent agreement with experimental results for $f = 4\%$ and demonstrate the ability of the model to capture the entire hysteresis responses fairly accurately based on the DMA characterization. It is to be noted that the model can predict the nonlinear viscous behavior accurately for a quite large strain value at 10%. In addition to that, to explore the predictive capability of the model at another volume fraction, a $f = 9\%$ PU–MTM nanocomposite is considered. It is assumed that the stiffnesses associated with the combined clay and interphase are increased by a factor of 2.25 in accordance with the increase in the clay content. The relaxation times are assumed to be same as for $f = 4\%$. Following Eq. (26) the rate of viscous damping for $f = 9\%$ will decrease compared to $f = 4\%$ as a function of the product $(G \times t_r)$ due to the increase in G values as the t_r remain the same, which is in accord with the understanding that viscous damping reduces in PU–MTM nanocomposites with increase in clay volume fraction. The FE model predictions for the quasi-static response at two different strain levels are plotted and compared against experimental data in Fig. 7 (b). A very accurate agreement is obtained between the FE predictions and experimental results.

Table 2
Material parameters corresponding to the constitutive model for the clay-interphase component of PU–MTM ($f = 4\%$).

i	1	2	3	4	5
$t_{ri}(sec)$	4.435	0.456	0.145	0.025	0.0028
$G_i(MPa)$	124	67	103	224	288
$G_0 = nk\theta$	30 MPa				
N	20				
k	$1.38 \times 10^{-20} N - mm/K$				
$S_{0,1}$	12.5 MPa				
$A_{0,1}$	2×10^{-20}				

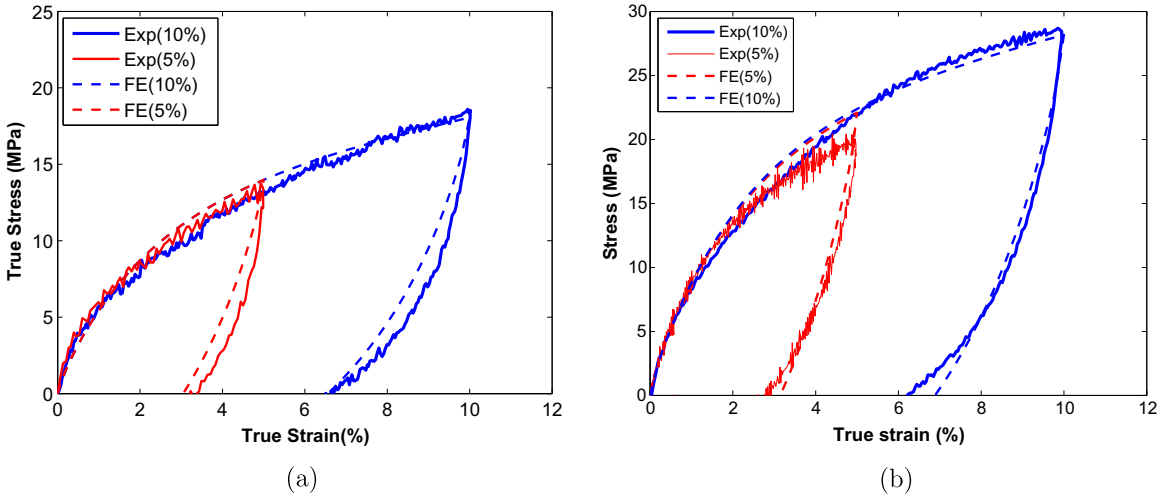

Fig. 7. Uniaxial loading–unloading response curves for PU–MTM nanocomposites at a quasi-static rate of 0.5% sec and model predictions at 5% and 10% strain for $f = 4\%$ (a) and for $f = 9\%$ (b).

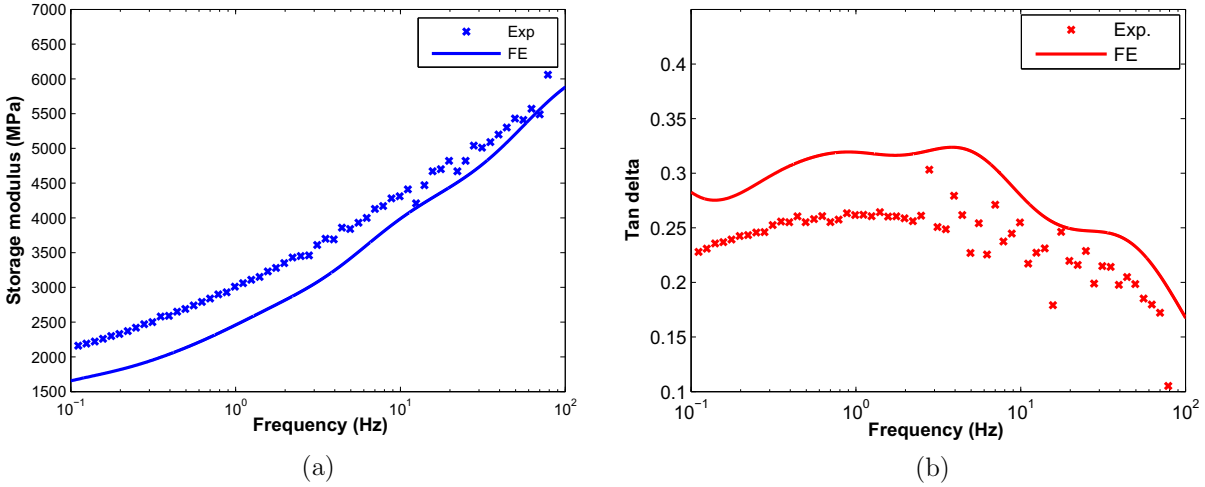

Fig. 8. Storage modulus versus frequency (a) and *tan δ* versus frequency (b) response curves and model predictions for $f = 9\%$ PU–MTM nanocomposites.

The frequency dependent storage modulus and tan δ are also predicted for $f = 9\%$ and compared with experimental DMA measurements as shown in Fig. 8. The predictions agree reasonably well with the experiments but in general underpredicts the stiffness and overpredicts the damping, specifically in the low frequency regime. Increased amounts of clay hinders relaxation properties of polymer chains and the resulting nanocomposite response transitions from a ductile to brittle behavior with a considerable reduction in damping, as reported in Kaushik et al. (2011). The slower relaxation times, which dominates the behavior at low frequency become even more slower with increased clay volume fraction. Hence in the present case, slower relaxation times (t_r) for the combined clay and interphase also might have altered at $f = 9\%$ compared to $f = 4\%$ along with the G values, which our current model has not considered due to the limitation in least square fitting of time constants. Hence the model predictions for the DMA data for $f = 9\%$ shows less stiff behavior for the nanocomposites compared to the experimental results.

5. Conclusions

A finite deformation rate dependent constitutive model is presented for PU and PU–MTM nanocomposites to characterize the frequency dependent mechanical responses of these materials. The PU model predicts the storage modulus versus frequency response as well as the rate and strain dependent loading–unloading response, based on nonlinear elastic and linear viscous characterization. It is shown that the frequency dependent damping characterization is effective at predicting the strain rate dependent response of PU up to approximately 10%/sec. Incorporation of nonlinear elasticity increases the accuracy of the model to predict the rate dependent response up to what is considered to be a fairly large strain (10%) for linear viscous materials. The present approach identifies the importance of faster relaxation times in polymers in order to predict high rate response accurately. Based on the constitutive description of PU, a phenomenological model was presented for PU–MTM nanocomposites, in which the clay particles and the interphase are treated as a homogenized material. A frequency sweep of the damping (tan δ) is used to fit the material parameters for $f = 4\%$, as in the PU model. The response of the $f = 9\%$ nanocomposite is predicted by assuming the moduli scale by the same ratio as the clay volume fraction. The predicted results are in excellent agreement with the loading–unloading response curves at two strain levels and there is reasonable agreement with the DMA data. The proposed methodology effectively predicts the strain dependent nonlinear viscous response of polymer nanocomposites in terms of both loading and unloading responses. The model predictions show very good agreement with experimental results for both PU and PU–MTM systems, for uniaxial loading–unloading responses at various strain levels.

Acknowledgement

The authors gratefully acknowledge the financial support provided by the Defense Advanced Research and Project Agency (DARPA) and the Office of Naval Research (ONR) (USA) to carry out this work. The contribution of Bret Kitcher, Mechanical Engineering Department at the University of Michigan, Ann Arbor, to carry out all the experiments for PU and PU–MTM samples, and Dr. Bongjun Yeom and Prof. Nicholas Kotov of the Chemical Engineering Department for their valuable guidance in manufacturing of the PU and PU–MTM samples, are greatly appreciated and acknowledged.

Appendix A. Summary of the stress update algorithm in ABAQUS VUMAT for PU

- Known at time t_n : $\mathbf{F}_n, \mathbf{F}^e_n, \mathbf{F}^v_n, \mathbf{T}_n, \overline{\tau_{v,n}}, \dot{\gamma}^v_{d\ n}$
  Given at time t_{n+1} : $\mathbf{F}_{n+1}$
- Using explicit forward Euler approach, the viscous flow rule (for the ith branch) is integrated as:

$$\mathbf{F}^v_{n+1} = \mathbf{F}^v_n + \left(\dot{\gamma}^v_{d\ n}\frac{1}{\sqrt{2}\overline{\tau_{v,n}}}\mathbf{T}^{e\prime}_n\right)\mathbf{F}^v_n\Delta t \tag{A.1}$$

  This step repeats for all the Maxwell branches.
- With $\mathbf{F}^v_{n+1}$ determined in the last step, elastic part of the deformation gradient for each Maxwell branch is computed as:

$$\mathbf{F}^e_{n+1} = \mathbf{F}_{n+1}\left(\mathbf{F}^v_{n+1}\right)^{-1} \tag{A.2}$$

- Perform eigenvalue decomposition on $\mathbf{F}^e_{n+1}$ to find out the stretch tensor $\mathbf{V}^e_{n+1}$
- Calculate the Cauchy stress as:

$$\mathbf{T}^e_{n+1} = \frac{1}{(det\mathbf{F}^e_{n+1})}\mathbf{L}^e\left(ln\mathbf{V}^e_{n+1}\right) \tag{A.3}$$

- Calculate the equivalent stress as:

$$\overline{\tau_{v,n+1}} = \left[\frac{1}{2}\mathbf{T}^e_{n+1\prime}\mathbf{T}^e_{n+1\prime}\right]^{1/2} \tag{A.4}$$

  where $\mathbf{T}^e_{n+1\prime} = \mathbf{T}^e_{n+1} - 1/3trace(\mathbf{T}^e_{n+1})$
- Update the viscous strain rate at $(n+1)$ th time step as:

$$\dot{\gamma}^v_{d\ n+1} = \frac{\sqrt{2}\tau_{v,\bar{n}+1}}{2Gt_r} \tag{A.5}$$

- To calculate the stress in the Arruda–Boyce spring, update the left Cauchy–Green strain as:

$$\overline{\mathbf{B}}_{n+1} = \overline{\mathbf{F}}_{n+1}\overline{\mathbf{F}}^T_{n+1} \tag{A.6}$$

- Calculate the stress in the Arruda–Boyce spring using Eq. (3) as:

$$\mathbf{T}^{n+1} = \frac{n_1 k\theta}{3J}\frac{\sqrt{N}}{\lambda_{chain,n+1}}L^{-1}\left(\frac{\lambda_{chain,n+1}}{\sqrt{N}}\right)\mathbf{B}^{\bar{}}_{n+1} \tag{A.7}$$

References

Anand, L., 1996. A constitutive model for compressible elastomeric solids. Comput. Mech. 18, 339–352.
Anand, L., 2003. A continuum theory of amorphous solids undergoing large deformations, with application to polymeric glasses. Tech. Rep. AMMNS-3660, Advanced Materials for Micro- and Nano-Systems (AMMNS), Singapore MIT Alliance.
Anand, L., Gurtin, M.E., 2003. A theory of amorphous solids undergoing large deformations, with applications to polymeric glasses. Int. J. Solids Struct. 40, 1465–1487.
Argon, A.S., 1973. A theory for the low temperature plastic deformation of glassy polymers. Philos. Mag. 28, 507–530.
Arruda, E.M., Boyce, M.C., 1993. Evolution of plastic anisotropy in amorphous polymers during finite straining. Int. J. Plast. 9, 697–720.
Arruda, E.M., Boyce, M.C., Jayachandran, R., 1995. Effects of strain rate, temperature and thermomechanical coupling on the finite strain deformation of glassy polymers. Mech. Mater. 19, 193–212.
Bergstrom, J.S., Boyce, M.C., 1998. Constitutive modeling of the large strain time dependent behavior of elastomers. J. Mech. Phys. Solids 46, 931–954.
Boyce, M.C., Parks, D.M., Argon, A.S., 1988. Large inelastic deformation of glassy polymers. part i: rate dependent constitutive model. Mech. Mater. 7, 15–33.
Coleman, J.N., Cadek, M., Blake, R., Nicolosi, V., Ryan, K.P., Belton, C., Fonseca, A., Nagy, J.B., Blau, W.J., 2004. High performance nanotube-reinforced plastics: understanding the mechanism of strength increase. Adv. Funct. Mater. 14, 791–798.
Haupt, P., Lion, A., BackHaus, E., 2000. Dynamic behavior of polymers under finite strains. Int. J. Solids Struct. 37, 3633–3646.

Kaushik, A.K., Waas, A.M., Arruda, E.M., 2011. A constitutive model for finite deformation response of layered polyurethane–montmorillonite nanocomposites. Mech. Mater. 43, 186–193.
Kheng, E., Iyer, H., Podsiadlo, P., Kaushik, A.K., Kotov, N., Arruda, E.M., Waas, A.M., 2010. Fracture toughness of exponential layer-by-layer polyurethane/poly(acrylic acid) nanocomposite films. Eng. Fract. Mech. 77, 3227–3245.
Li, Y., Waas, A.M., Arruda, E.M., 2011a. A closed-form hierarchical multi-interphase model for composites-derivation, verification, and application to nanocomposites. J. Mech. Phys. Solids 59, 43–63.
Li, Y., Waas, A.M., Arruda, E.M., 2011b. The effects of the interphase and strain gradients on the elasticity of layer by layer (LBL) polymer/clay nanocomposites. Int. J. Solids Struct. 48, 1044–1053.
Lion, A., 1998. Thixotropic behavior of rubber under dynamic loading histories: experiments and theory. J. Mech. Phys. Solids 46, 895–930.
Liu, H., Brinson, L.C., 2006. A hybrid numerical–analytical method for modeling the viscoelastic properties of polymer nanocomposites. J. Appl. Mech. Trans. ASME 73, 758–768.
Mulliken, A.D., Boyce, M.C., 2006. Mechanics of the rate dependent elastic–plastic deformation of glassy polymers from low to high strain rates. IJSS 43, 1331–1356.
Muzny, C.D., Butler, B.D., Hanley, H.J.M., Tsvetkov, F., Peiffer, D.G., 1996. Clay platelet dispersion in a polymer matrix. Mater. Lett. 28, 379–384.
Nguyen, Q.T., Baird, D.G., 2006. Preparation of polymer–clay nanocomposites and their properties. Adv. Polym. Technol. 25, 270–285.
Podsiadlo, P., Kaushik, A.K., Arruda, E.M., Wass, A.M., Shim, B., Xu, J., Nandivada, H., Pumplin, B.G., Lahaan, J., Ramamoorthy, A., Kotov, N.K., 2007. Ultrastrong and stiff layered polymer nanocomposites. Science 318, 80–83.
Qi, H.J., Boyce, M.C., 2005. Stress–strain behavior of thermoplastic polyurethanes. Mech. Mater. 37, 817–839.
Ramanathan, T., Liu, H., Brinson, L.C., 2005. Functionalized SWNT polymer nanocomposites for dramatic property improvement. J. Polym. Sci. Part B: Polym. Phys. 43, 2269–2279.
Sandler, J.K.W., Shaffer, M.S.P., Prasse, T., Bauhofer, W.K., Windle, A.H., 1999. Development of a dispersion process for carbon nanotubes in an epoxy matrix and the resulting electrical properties. Polymer 40, 5967–5971.
Sheng, N., Boyce, M.C., Parks, D.M., Rutledge, G.C., Abes, J., Cohen, R.E., 2004. Multiscale micromechanical modeling of polymer/clay nanocomposites and the effective clay particle. Polymer 45, 487–506.
Shim, J., Mohr, D., 2011. Rate dependent finite strain constitutive model of polyurea. Int. J. Plast. 27, 868–886.
Wineman, A.S., Rajagopal, K.R., 2000. Mechanical Response of Polymers: An Introduction. Cambridge University Press.